Benthic biolayer structure controls whole-stream reactive transport

Kevin R. Roche[1,2], **Marco Dentz** [1]

[1]Spanish National Research Council (IDAEA-CSIC), Barcelona, Spain
[2]Department of Civil Engineering, Boise State University
[1]c/ Jordi Girona, 18, 08034 Barcelona, Spain
[2]1910 University Dr, Boise, ID 83725, USA

Key Points:

- Timescales of transport through, and reaction within, the benthic biolayer determine rates of whole-stream reactions.
- Biolayer structure determines timescales that reactive solutes will persist in the stream.
- New mobile-immobile model provides analytical predictions of local- and whole-stream reactive transport.

Corresponding author: Kevin R. Roche, `kevinrroche@boisestate.edu`

Abstract

Hyporheic zone reaction rates are highest just below the sediment-water interface, in a shallow region called the benthic biolayer. Vertical variability of hyporheic reaction rates leads to unexpected reaction kinetics for stream-borne solutes, compared to classical model predictions. We show that deeper, low-reactivity locations within the hyporheic zone retain solutes for extended periods, which delays reactions and causes solutes to persist at higher concentrations in the stream reach than would be predicted by classical models. These behaviors are captured by an upscaled model that sheds light on the fundamental physical and chemical processes in the hyporheic zone, and how the time scales of transport and reaction within the biolayer control solute retention and transformation at the scale of the entire stream.

Plain Language Summary

Dissolved materials such as carbon, nutrients, and contaminants react as they move through the river network. Some locations in the river are far more reactive than others, and it is challenging to predict how this spatial variability of reaction rates controls the reactivity of the entire stream. One hotspot of high reactivity is the benthic biolayer, a thin region below the sediment-water interface with an abundance of microbial activity, and below which reactivity commonly decrease to very low values. We use a mathematical model to quantify the benthic biolayer's contribution to whole river material transformation, based on the biolayer's thickness and reactivity. We also show that thin or less reactive biolayers allow dissolved mass to become sequestered for long periods deep in the streambed, leading to low but persistent concentrations long after the mass is introduced to the river. These theoretical advances improve our understanding of how measurable features of the river - namely, the depth-dependent reaction rates within the streambed - are directly related to river biogeochemistry at larger scales. They may also improve estimates for how long trace contaminants may persist above toxicity thresholds in streams and rivers, since these contaminants may adversely impact river ecosystems at extremely low concentrations.

1 Introduction

A defining feature of rivers is the transition in physical and chemical characteristics across the sediment-water interface (SWI). Downstream velocities, mixing rates, and light availability decrease rapidly at the SWI to viscous flows and light limited conditions. This transition zone is called the benthic biolayer due to the large amount of microbial biomass and biogeochemical reactivity relative to other regions of the stream, and it contributes disproportionately to the heterotrophic respiration of carbon, nutrient cycling, and contaminant sequestration. Surface water exchanged with the the biolayer is high in oxygen relative to other regions of the streambed, which favors heterotrophic microbial biofilms with high metabolism (Battin et al., 2016). Dissolved oxygen depletes as water propagates deeper into the hyporheic zone (HZ) or further along advective flow paths, leading to conditions that sustain microbial communities with higher tolerance for anoxia and slower metabolism. This stratification of chemical conditions and microbial biomass in the benthic biolayer creates gradients in reaction rates over scales as little as millimeters, which poses a persistent challenge for measuring and modeling the hyporheic zone's contribution to whole stream reactive transport (Krause et al., 2017).

The profile of reaction rates within the biolayer is commonly inferred using a combination of concentration depth profiles and reactive transport modeling (e.g., O'Connor & Harvey, 2008). Inference is not only challenging because it is difficult to measure high concentration gradients in the subsurface, but also because myriad transport processes are simultaneously active (e.g., advective pumping, molecular and turbulent diffusion, mechanical dispersion). These processes are often grouped using scaling laws to predict

net water fluxes across the SWI. Predictions are related to subsurface concentrations by assuming that solutes diffuse vertically (O'Connor & Harvey, 2008; Grant et al., 2012; Voermans et al., 2018). The simplicity of the effective diffusion representation allows spatially-variable reaction rates to be inferred in the subsurface, typically via fits of concentration profiles to a reaction diffusion model or similar 1-D transport model (J. W. Harvey et al., 2013; Knapp et al., 2017; Schaper, Posselt, et al., 2018).

Stream-scale transformation rates directly depend on the spatial variability of reaction rates in the benthic biolayer, which underscores the need for whole-scale reactive transport models that account for these variations. For example, numerical simulations show that whole-stream transformation is 5-25× greater when HZ reaction rates are highest near the SWI, compared to a stream with reactions uniformly distributed in the HZ (Li et al., 2017). These differences arise because solutes entering the HZ typically propagate through shallow, high reactivity flowpaths before returning to the water column. Process-based models must therefore account for the correlation between reaction probability and residence time in the HZ. Models for advection-dominated hyporheic flows have accounted for these correlations, since decreasing reaction rates along hyporheic flowpaths can be mapped to temporal increments of the hyporheic residence time distribution (Azizian et al., 2015; Reeder et al., 2018). However, a similar space-for-time mapping is more challenging when hyporheic transport is represented as a diffusive process, and we currently lack an upscaling framework that accounts for both spatially varying reaction rates and the random nature of diffusive transport.

In this study, we isolate the effects of depth-dependent HZ reaction rates on upscaled predictions of solute fate in a river. Solute transport in the HZ is considered to be dominated by vertical diffusion, which aligns our analysis with existing diffusion-based scaling laws that predict hyporheic exchange fluxes from measurable stream parameters. We present streambed-scale and reach-scale simulations designed to mimic a pulse tracer injection, which is a common method for assessing the processes controlling reactive transport in rivers. Numerical results are compared to predictions from a classical mobile-immobile model with uniform reactions in the subsurface, as well as predictions from a novel mobile-immobile model that explicitly represents the vertically-varying reaction profile in the biolayer. This work is motivated by the questions of how the size, shape, and reactivity of the benthic biolayer influence reach-scale mass fate, and how these properties manifest in upscaled observations of reactive transport.

2 Methods

W describe transport and reaction scenarios under consideration. We then present a novel mobile-immobile biolayer model, which we use to determined equivalent streambed and reach scale reactivities. Finally, we describe the method used for the direct numerical simulations of transport and reaction in the combined river-HZ system.

2.1 Transport scenario

The concentration of a solute in the river-HZ system is governed by the advection-dispersion equation

$$\frac{\partial C}{\partial t} + v(z)\frac{\partial C}{\partial x} - \frac{\partial}{\partial z}\left[D(z)\frac{\partial}{\partial z}C\right] = -k(z)C. \tag{1}$$

The SWI is located at $z = 0$. The water column velocity is defined as $v(z) = \overline{v}+v_0\kappa^{-1}(1+\ln zd^{-1})$ for $0 < z < d$, where d is depth of the water column, $\kappa \approx 0.41$ is the von Karman coefficient (Fischer et al., 1979), and v_0 is the shear velocity. Streamwise velocity is set to $v(z) = 0$ for $z \leq 0$, which assumes that the velocity in the HZ is negligible compared to the velocity of the river. The vertical dispersion coefficient is $D(z) = \kappa v_0 z(1 - zd^{-1})$ for $z > \epsilon$ and $D(z) = D_h$ for $-h < z < \epsilon$, where D_h is the diffusion

coefficient and h the depth of the HZ. The horizontal boundaries are impermeable. In line with experimental design of field tracer studies, we assume that the HZ is initially free of reactive mass, and solute is introduced as a line injection in the water column.

Solutes undergo first-order reactions in the HZ, which is a reasonable assumption when the modeled solute is limiting, meaning reactions are independent of the concentration of co-reactants, abundance of catalysts such as enzymes, or thermodynamic constraints (Dodds et al., 2002; Garayburu-Caruso et al., 2020). The depth-dependent reaction rate $k(z)$ can be an arbitrary function of streambed elevation $z \leq 0$, but typically decreases sharply with depth. We follow Li et al. (2017) and consider a layer structure consistent with field observations (Knapp et al., 2017; Schaper, Posselt, et al., 2018; Inwood et al., 2007; O'Connor & Harvey, 2008), that is, $k(z) = k_b \mathbb{I}(-b < z < 0)$, where the impulse function $\mathbb{I}(\cdot)$ is 1 if the argument is true and 0 otherwise. The reaction rate is equal to k_b for $-b < z < 0$ with b the depth of the benthic layer, see Figure 1. Other profiles that decay on a characteristic length scale b are expected to show a qualitatively similar behavior. To generalize our results across all profile shapes, we define a biolayer Damköhler number as $Da = \tau_b k_b$ where $\tau_b = b^2 D_h^{-1}$ is the characteristic diffusion time over the benthic biolayer. The model is summarized in Figure 1. We focus on quantifying the system reactivity and downstream breakthrough curves.

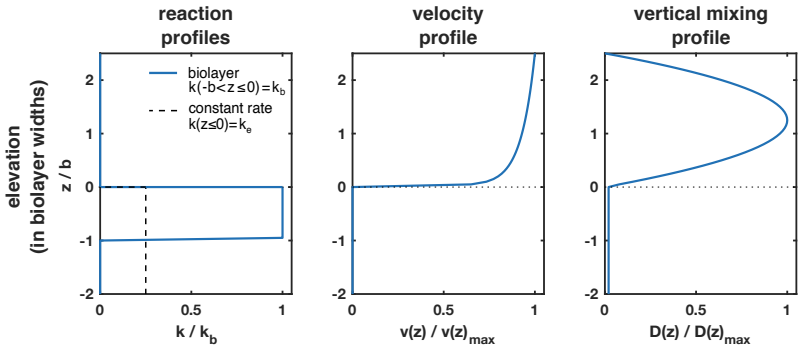

Figure 1. (Left to right) Spatial reaction, velocity and vertical mixing profiles across the surface-subsurface continuum. The SWI is $z = 0$.

2.2 Upscaled mobile-immobile biolayer (MIM-B) model

To upscale the reactive transport problem, we employ a dual porosity approach (Villermaux, 1974; Haggerty & Gorelick, 1995; Boano et al., 2007). Equation (1) is decomposed into an advection-dispersion equation for the stream concentration C_s, and a diffusion-reaction equation for C_H in the HZ. These equations are coupled through concentration and flux continuity at $z = 0$. Vertical averaging over the water column gives

$$\frac{\partial}{\partial t}\left(\overline{C}_s + \frac{1}{d}M_h\right) + \overline{v}\frac{\partial}{\partial x}\overline{C}_s - D^*\frac{\partial^2}{\partial x^2}\overline{C}_s = -\frac{1}{d}k_b M_b, \tag{2}$$

where $\overline{C}_s$ is the vertically averaged stream concentration, M_h the mass in the HZ, M_b the mass in the biolayer, and $D^* = 5.93 v_0 d$ is the shear dispersion coefficient (Fischer et al., 1979). Details are given in the supporting information. The masses M_h and M_b are related to $\overline{C}_s$ via the linear relation

$$M_j = \int_0^t \mathrm{d}t' \, \varphi_j(t - t')\overline{C}_s(t') \tag{3}$$

with $j = h, b$. The memory functions $\varphi_h(t)$ and $\varphi_b(t)$ describe the evolution of mass in the HZ and in the biolayer in response to an instantaneous solute pulse at the SWI, which can be seen by setting $\overline{C}_s(t') = \delta(t')$ in (3). Similarly, the mass M_0 in the hyporheic sublayer, which is the region below $z = -b$, is related to $\overline{C}_s$ through the memory function φ_0. The memory function φ_h is given by the sum $\varphi_h(t) = \varphi_b(t) + \varphi_0(t)$. Details on the derivation of these relations and explicit Laplace space expressions for φ_b, φ_0 and φ_h are given in supporting information.

2.3 Equivalent reactivities

We define equivalent reactivity on the scale of the streambed and on the reach scale such that an equivalent model with a constant reaction rate produces the same reacted mass as the biolayer scenario.

2.3.1 Reactivity in streambed

We consider a constant reaction profile $k(z) = k_e$ in the hyporheic zone. In this case, $M_b = M_h \equiv M_e$ in (2) so that the equation for $\overline{C}_s$ reads as

$$\frac{\partial}{\partial t}\left(\overline{C}_e + \frac{1}{d}M_e\right) + \overline{v}\frac{\partial}{\partial x}\overline{C}_e - D^*\frac{\partial^2}{\partial x^2}\overline{C}_e = -\frac{1}{d}k_e M_e, \tag{4}$$

The streambed concentration predicted by this model is denoted by $\overline{C}_e$. The memory function $\varphi_h(t) = \varphi_b(t) \equiv \varphi_e(t)$ is given by $\varphi_e(t) = \phi(t)\exp(-k_e t)$, where $\phi(t)$ is the memory function for a conservative solute. Explicit Laplace space expressions for $\phi(t)$ and $\overline{C}_e(t)$ are given in supporting information. We refer to this model as the mobile-immobile constant reactivity (MIM-C) model.

The effective reaction rate k_e in (4) is defined such that the total reacted mass in the HZ in response to an instantaneous pulse at the SWI are equal in the biolayer scenario and the surrogate scenario described by (4). This means

$$k_e \int_0^\infty \mathrm{d}t\, \varphi_e(t) \equiv k_b \int_0^\infty \mathrm{d}t\, \varphi_b(t). \tag{5}$$

Using this relation, we derive in the supporting information the streambed-scale equivalent reactivity k_e:

$$\sqrt{\frac{k_e}{k_b}}\tanh\left(\sqrt{k_e\tau_h}\right) = \tanh\left(\sqrt{Da}\right), \tag{6}$$

where $\tau_h = h^2 D_h^{-1}$ is the characteristic diffusion time across the HZ. The solution of (6) can be approximated by $k_e = k_b \tanh\left(\sqrt{Da}\right)^2$ for $k_e\tau_h > 10$.

2.3.2 Reactivity at the reach scale

In order to define an equivalent reach scale reactivity, we write a single-domain equation for the streambed concentration characterized by the constant reactivity k_r as

$$\frac{\partial}{\partial t}\overline{C}_r + \overline{v}\frac{\partial}{\partial x}\overline{C}_r - D^*\frac{\partial^2}{\partial x^2}\overline{C}_r = -k_r\overline{C}_r. \tag{7}$$

The river concentration predicted by this model is denoted by $\overline{C}_r$. Reach scale reactivity is defined such that the total mass reacted in the reach up to a distance x from the injection point is equal in the biolayer scenario and the single domain surrogate scenario (7). This implies

$$k_r \int_0^\infty \mathrm{d}t \int_0^x \mathrm{d}x'\, \overline{C}_r(x', t) \equiv k_b \int_0^\infty \mathrm{d}t \int_0^x \mathrm{d}x'\, \overline{C}_s(x', t) \tag{8}$$

Using the explicit analytical expressions for $\overline{C}_r$ and $\overline{C}_s$ given in the supporting information, we obtain for the reach scale reactivity

$$k_r = \frac{\overline{v}^2}{2D^*}\left(\sqrt{1+\frac{4D^*\sqrt{k_b D_h}\tanh(\sqrt{Da})}{d\overline{v}^2}}-1\right). \tag{9}$$

Note that the single domain model (7) characterized by the reaction rate (9) has the same longitudinal profile of total reacted mass as the combined stream-streambed scenario, which is given by $M_r(x) = \exp(-k_r x\overline{v}^{-1})$. This predicted exponential decrease is commonly observed in field experiments and is related to other common metrics of whole-stream reactivity. Namely, $\overline{v}k_r^{-1}$ is the nutrient spiraling length that describes the characteristic distance a reactive molecule travels downstream before reacting (Tank et al., 2017), and $\exp(-k_r x\overline{v}^{-1})$ is the reaction significance factor, which describes the cumulative fraction of removal within the reach (J. Harvey et al., 2019).

2.4 Numerical simulations

The advection-dispersion equation (1) is solved numerically using a reactive time-domain random walk approach (TDRW), based on the implementation of Russian et al. (2016) for conservative solutes. The TDRW method is computationally efficient for media with heterogeneous advection, diffusion and reaction properties. The grid resolution is set to $\Delta z = \min(10^{-2}\,\mathrm{m}, 10^{-1}b)$. To ensure that our results are consistent with continuum assumptions in our analytical model, we restrict our analysis to times greater than the characteristic residence time in a single grid cell.

2.4.1 Reactivity in the streambed

Streambed-scale experiments were used to characterize the temporal evolution of reactive solute retained in the HZ for an instantaneous solute pulse at the stream-streambed interface. We set a no-flux boundary at $z = -h$, an absorbing boundary at $z = 0$ for $t > 0$, and released a pulse of N_0 particles in the first grid cell below $z = 0$ at $t = 0$. We then determined the evolution of the total number of particles in the biolayer, the sublayer and the full HZ, which is equivalent to the respective memory functions.

2.4.2 Reactivity at the reach scale

Reach-scale simulations were designed to mimic a pulse tracer injection commonly performed in field experiments. We release N_0 particles uniformly in the mobile zone at $x = 0$ m and $t = 0$ s. Breakthrough curves are given by the distribution of particle arrival times at a downstream distance x in the stream.

3 Results and discussion

3.1 Scales and processes in the streambed

We first discuss processes and the related time scales for reaction and diffusion in the streambed in order to shed light on the interplay between biolayer structure, and retention and diffusion processes. Recall that the memory functions denote the mass in the HZ in response to an instantanous solute pulse at the SWI. Figure (2) shows the memory function for (a) the sublayer, (b) the biolayer, and (c) the entire HZ.

We consider the following order of time scales, $\tau_R < \tau_b \leq \tau_\ell$, where $\tau_\ell = \ell^2/D$ is the diffusion time across the sublayer of dimension $\ell = b - h$, and $\tau_R = k_b^{-1}$ is the reaction time. This means reactions occur before solute is transmitted to the sublayer. If $\tau_R > \tau_b$ only a small amount of mass reacts before it propagates through the benthic biolayer. In this case, the behaviors of the reactive memory functions are very sim-

ilar to the one for conservative transport. The memory function $\varphi_0(t)$ shown in Figure 2a, describes solute retention in the nonreactive sublayer. It increases from 0 to a maximum on the time scale τ_b, which is the time for solute transmission across the biolayer. It then decreases as $t^{-1/2}$, as for a conservative solute, due to diffusion back to the biolayer. Last, it tempers exponentially on the time scale τ_ℓ as the sublayer depletes by diffusion. The memory function φ_b for the biolayer decays as $t^{-1/2}$ for $t \ll \tau_R$, that is, at times smaller than the reaction time. The mass in the biolayer is depleted as solute diffuses below, and reacts within, the biolayer (Figure 2b). The timescale of depletion is controlled by the relative magnitudes of τ_b and τ_R, with more depletion occurring for fast reactions or for deep biolayers (i.e., $Da \gg 1$). For times $t \gg \tau_b$, mass is well mixed across the biolayer, and φ_b transitions to a $t^{-3/2}$ decay because mass in the biolayer changes in a quasi-static fashion due to the mass flux from the sublayer (see supporting information),

$$\varphi_b(t) = -\frac{\tau_b}{1+Da}\frac{\mathrm{d}\varphi_0}{\mathrm{d}t} \propto t^{-3/2}. \tag{10}$$

The memory function φ_h integrates the diffusion-reaction process in the biolayer and retention in the sublayer (Figure 2c). For times $t \ll \tau_R$, mass removal in the streambed is primarily caused by diffusion upward across the SWI, and we observe the characteristic $t^{-1/2}$ decay of a conservative solute. As discussed above, solute is depleted by reaction in the biolayer for $t > \tau_R$, leading to an exponential decay of φ_h. For $t < \tau_b$ all remaining mass resides at shallow depth in the benthic biolayer, and the system behaves identically to a scenario of constant streambed reactivity. For for $t > \tau_b$, however, solute diffuses into the inert sublayer. Eventually, most mass remaining in the streambed is sequestered below the biolayer (Figure 2a,b), after which the upward diffusion of mass from the inert sublayer into the biolayer results in a second regime of $\varphi_h(t) \sim t^{-1/2}$ (Figure 2c) because diffusion from the sublayer through the biolayer and to the stream is the dominant depletion process. Exponential tempering of $\varphi_h(t)$ then occurs on the time scale τ_ℓ (Figure 2c). For comparison, we show memory functions for the corresponding MIM-C model parameterized with k_e. It decays as $t^{-1/2}$ for times smaller than the reaction time $\tau_e = k_e^{-1}$ and exponentially fast for $t > \tau_e$ as solute is degrades throughout the HZ. Thus, the MIM-C model predicts much faster depletion of reactant than the MIM-B model because it does not account for long survival in the sublayer.

In summary, the interaction of reaction and diffusion processes in the HZ is governed by three distinct timescales: the characteristic reaction time $\tau_R = k_b^{-1}$, which sets the time for reactive solute depletion from the biolayer; the diffusion time τ_b, which sets the time for solution transmission through the biolayer to the inert sublayer; and τ_ℓ, which marks the time for diffusive depletion of solute from the HZ.

3.2 Reach-scale observations and model predictions

3.2.1 Effective streambed- and reach-scale reactivity

The theoretical prediction (6) of k_e agrees well with estimates from streambed numerical experiments, showing that Da strongly controls k_e (Figure 3a). The plot also shows that k_e and k_b are identical when $Da \gg 1$, meaning spatial variability of $k(z)$ has little bearing on effective streambed reactivity in these cases. To understand this, note that $Da^{1/2} = bs^{-1}$, where $s = (D_h/k_b)^{1/2}$ is the characteristic survival depth of reactive solute that enters the streambed at the SWI. When $b \gg s$ (i.e., $Da \gg 1$), nearly all solute reacts before propagating below the biolayer. In contrast, a substantial amount of mass propagates through the biolayer unreacted when $b < s$ (i.e., $Da < 1$), reducing effective reactivity to a fraction of that for a fully reactive streambed, $k_e/k_b < 1$.

The similar shapes of the plots in Figures 3a and 3b demonstrate that the biolayer structure's influence on effective reach-scale reactivity k_r mirrors its influence on effective streambed reactivity. We show in Figure 3b the value of k_r normalized by k_r^h, the value of k_r for $b = h$, as a function of Da. The plot increases monotonically with in-

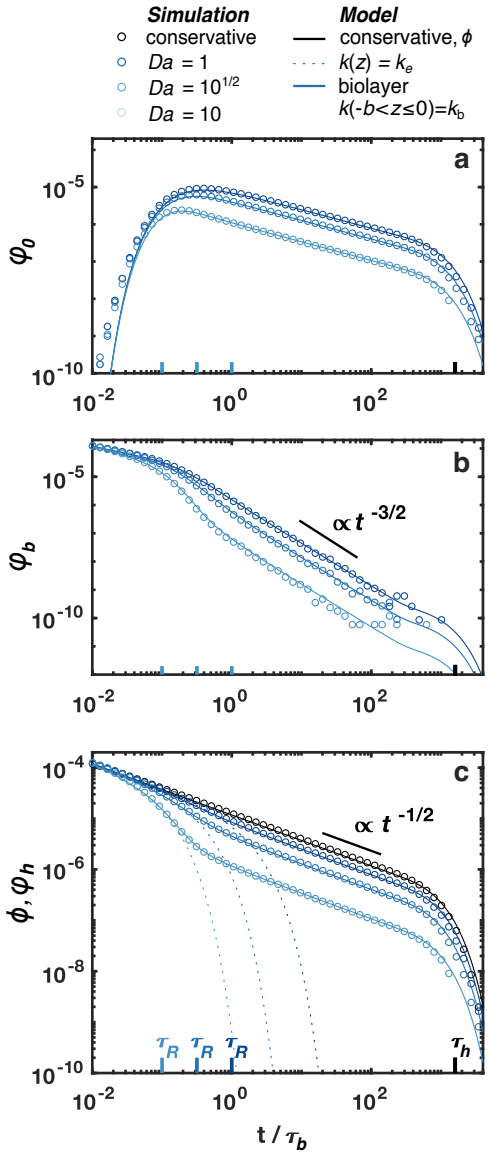

Figure 2. Modeled and simulated memory functions of varying biolayer Da. a) Memory functions for the inert sublayer show all mass in $-h \leq z < b$. b) Memory functions for the benthic biolayer show all mass in $-B \leq z < 0$. c) Full memory functions for conservative (black) and reactive (colored) solutes. Model and simulations transition to $t^{-1/2}$ tailing beyond the timescale specified in Eq. 10. Time is re-scaled by the biolayer diffusion time, τ_b.

creasing Da and assumes the value 1 for $Da = Da_h = \tau_h k_b$. The reach scale reactivity is always smaller than k_b because no reactions are modeled in the water column, which reduces the reactivity of the full stream-streambed system below k_b. Note that k_r, given by (9), is not a function of Da alone, but depends on the properties of the stream, as well as the diffusion coefficient D_h and reaction rate k_b explicitly. For realistic parameter values, expression (9) can be simplified to $k_r = k_b b(d\sqrt{Da})^{-1}\tanh(\sqrt{Da})$ because the second term under the square-root is much smaller than one.

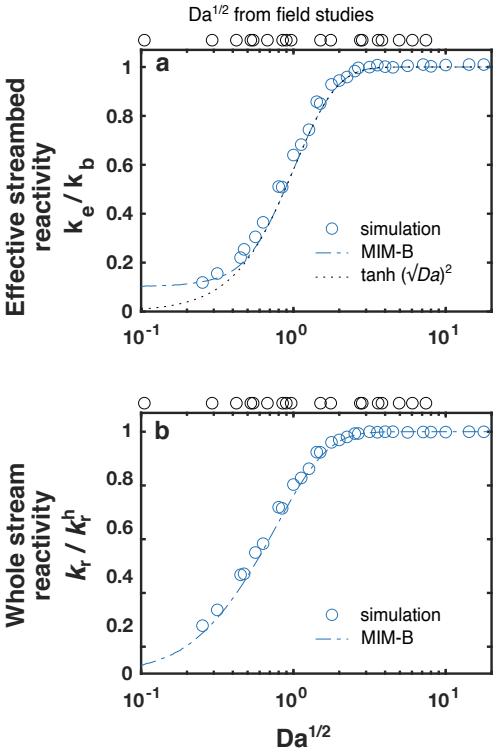

Figure 3. Measured and modeled reactivity across simulations and scales. a) Effective reaction rates for a streambed containing a biolayer. b) Whole-stream reactivity. Values are normalized by k_r^h, representing a HZ with $k(z) = k_b$. Results are compared to estimates of Da from Knapp et al. (2017); Li et al. (2017); Schaper, Seher, et al. (2018), shown as black circles above plots. See supporting information.

3.2.2 Breakthrough curves

Figure 4 shows tracer breakthrough curves in response to an instantaneous solute injection in the stream obtained from numerical simulations, the theoretical upscaled biolayer model and the surrogate models characterized by the constant reactivities k_r and k_e at reach scale and in the streambed. We consider scenarios for which τ_b and τ_R are much smaller than τ_h. The upscaled model fully captures the numerical BTCs, which are characterized by strong late time tailing as $t^{-3/2}$ and exponential tempering at the diffusion time scale τ_h. This tailing results from long-term solute retention in the inert sublayer, which allows trace amounts of solute to persist far longer in the reach than in cases where the entire HZ is reactive. Tail concentrations decrease with increasing Da because the amount of tracer that is removed in the bioloayer increases. However, the power-law decay in time due to diffusion in the inert sublayer persists. The surrogate models severely underpredict this late time tailing because they do not account for the reaction delay associated with mass sequestration below the biolayer. They predict an exponential decrease of tracer concentration on the time scales k_e^{-1} and k_r^{-1}, respectively. Consequently, simulated BTC concentrations exceed predictions from the constant rate models by multiple orders of magnitude at late times. In contrast, the theoretical predictions from the MIM-B model agree with the simulated BTCs over all times.

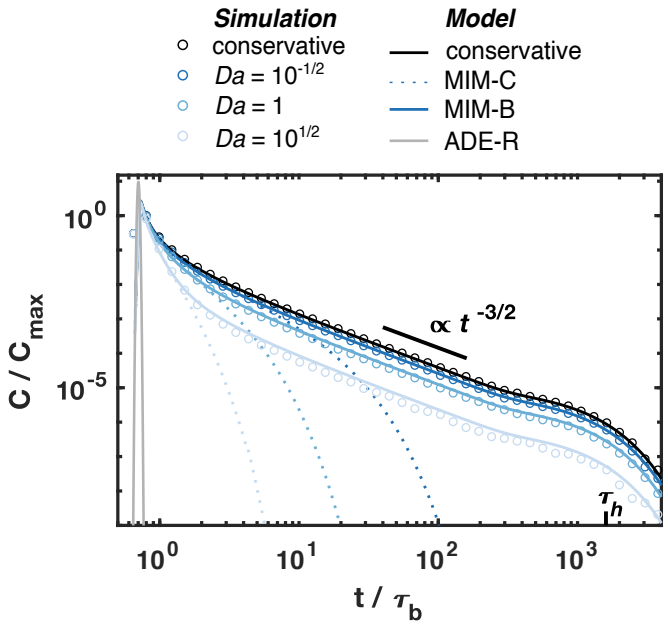

Figure 4. Breakthrough curves of conservative and reactive solutes for a pulse tracer injection$x = 250$ m, $d_H = -2$ m, and $b = 0.05$ m. Dotted lines represent the MIM-C model with constant HZ reactivity (Eq. 4), which does not accurately predict power-law tailing for $t > t_b$. Gray line is the ADE-R solution with reaction rate k_r (Eq. 7), for $Da = 10^{1/2}$; plots for ADE-R solutions at other Da are similar and are therefore omitted.

4 Implications

Even when reaction rates are high within the biolayer, solutes accumulate in the inert sublayer. Sequestration within, and slow diffusion from, the inert sublayer leads to a long time interval in which solute concentrations in the stream decay as a power law. During this time, concentrations within the streambed and at the reach scale greatly exceed predictions from models that assume solutes react uniformly within the HZ, as illustrated by the comparison to the MIM-C model in Figure 4 (dotted lines). In contrast, MIM-B captures the slow decrease of reactive solute within the streambed and reach. Comparisons between the analytical model and numerical simulations are nearly exact.

Our results show that representing spatially variable reaction rates in sediments is important for determining the temporal dynamics of trace chemical concentrations in both streambeds and in streams. Improved analytical methods have demonstrated the near-ubiquitous presence of anthropogenic organic contaminants in fresh waters (Bernhardt et al., 2017), which persist in sediments long after they enter the river network (Ciparis et al., 2012; Cozzarelli et al., 2017). Many of these chemicals impair stream ecosystems at low levels, such as endocrine disrupting compounds known to alter fish physiology at nanomolar concentrations (Adeel et al., 2017; Khanal et al., 2006). Microbial degradation of trace organic compounds is commonly highest in oxic porewaters within the biolayer that support high microbial metabolism. For example, the black markers above plots in Figure 3 include results from Schaper, Seher, et al. (2018), who observed a rapid decrease of trace organic contaminant degradation rates at the depth where hyporheic oxygen concentrations transitioned from oxic to anoxic levels. Many of these compounds have sufficiently low half lives to allow them to persist in deeper, low reactivity regions of the streambed, where they can eventually diffuse back into the biolayer and the stream (i.e., $Da < 1$). When complemented with measurements of redox gradients in the HZ,

the MIM-B model may therefore give realistic estimates of how long contaminants will persist at concentrations above toxicity thresholds.

Physical characteristics of the benthic biolayer are explicitly represented in the analytical expression for k_r (Eq. 9), thereby providing a direct mapping of biolayer structure to whole stream reactivity. The MIM-B therefore sheds light on the physical controls of stream-scale reactivity, which is a common motivation in studies of stream biogeochemistry and stream ecology (Pia-Ochoa & lvarez Cobelas, 2006; J. W. Harvey et al., 2013; Knapp et al., 2017). These studies often combine reach-scale tracer experiments with local physical experiments to distinguish which measurable stream characteristics control whole-stream mass transformation. This approach can be augmented by using the analytical predictions of whole-stream transformation from the MIM-B, based on local estimates of streambed reaction rates. For example, benthic chambers and sediment assays of denitrification potential are commonly used to estimate in situ nutrient uptake rates at the SWI, or k_b (Fellows et al., 2006; Findlay et al., 2011). These estimates could be combined with depth-based measurements or sediment assays in the HZ to determine the reaction profile $k(z)$ (Inwood et al., 2007; Knapp et al., 2017; Schaper, Seher, et al., 2018). Together with estimates of water column velocity and dispersion, these measures comprise the parameters needed to estimate the benthic biolayer's contribution to k_r using the MIM-B, which can be directly compared to stream tracer experiments.

We assume solute mixing is proportional to local concentration gradients in the streambed so that model assumptions agree with scaling laws relating hyporheic exchange fluxes to an effective diffusion coefficient D_e (Voermans et al., 2018). These semi-analytical scaling laws provide useful predictions of hyporheic exchange based on physical measurements (e.g., grain diameter, water column velocity) over a wide range of transport mechanisms (e.g., advective pumping, molecular and turbulent diffusion). By assuming the 1-D diffusion model is valid over shallow depths in the HZ, past studies have inferred $k(z)$ from chemical profile measurements in the benthic biolayer (O'Connor & Harvey, 2008). By providing closed-form analytical predictions of reach-scale reactivity using the same transport framework, we demonstrate the potential for extending these scaling laws to estimates of whole stream reactivity over the same range of transport mechanisms.

5 Conclusion

Two fundamental challenges for providing mechanistic predictions of river corridor reactivity are to explicitly link local heterogeneity of the controlling physical processes to upscaled observations within a consistent modeling framework, and to identify the relative importance of specific processes and structural features of the river (Ward & Packman, 2019; Kelleher et al., 2019). We address these challenges by quantifying how the benthic biolayer's structural features control overall stream reactivity and degradation timescales in the HZ. We identify the dominant physical and chemical processes in the HZ and their associated timescales, namely the reaction time in the biolayer, the diffusion time across the biolayer, and the storage time in the inert sublayer. Even for strongly reactive biolayers characterize by high Da, solute accumulation in the sublayer leads to long survival times characterized by an algebraic decay law of solute mass. These observations are critical for assessing contamination levels that can be dramatically underestimated by surrogate models that assume uniform reaction rates throughout the HZ.

The newly derived MIM-B model explicitly accounts for the interplay physical and chemical processes in the biolayer, thereby capturing all aspects of the reaction and transport behaviors at the streambed and reach scales. Furthermore, it provides expressions for streambed and reach scale reaction rates that are explicit functions of biolayer structure and reactivity. The MIM-B model therefore enables evaluation of the benthic biolayer's contribution to whole-stream reactive transport compared to alternative controlling mechanisms, including stream turbulence, diel temperature fluctuations, shear-

induced hyporheic mixing, and sorption-desorption (Grant et al., 2018; Zheng & Cardenas, 2018; Bandopadhyay et al., 2018; Cheng et al., 2021). The demonstrated link between the biolayer and reach-scale reactivity, presented here, further suggests that current scaling laws for hyporheic exchange flux may be extended to predict whole-stream mass transformation over a range of transport mechanisms.

Acknowledgments

KRR was supported by a junior scholar fellowship to Spain from the Fulbright Program. M.D. acknowledges the support of the Spanish Ministry of Science and Innovation (project HydroPore PID2019-106887GB-C31). Numerical data generated for this publication is based on the model of Russian et al. (2016), as described in the main text and supporting information.

References

Adeel, M., Song, X., Wang, Y., Francis, D., & Yang, Y. (2017, February). Environmental impact of estrogens on human, animal and plant life: A critical review. *Environment International*, *99*, 107–119. Retrieved 2020-06-10, from http://www.sciencedirect.com/science/article/pii/S0160412016304494 doi: 10.1016/j.envint.2016.12.010

Azizian, M., Grant, S. B., Kessler, A. J., Cook, P. L. M., Rippy, M. A., & Stewardson, M. J. (2015, September). Bedforms as Biocatalytic Filters: A Pumping and Streamline Segregation Model for Nitrate Removal in Permeable Sediments. *Environmental Science & Technology*, *49*(18), 10993–11002. Retrieved 2020-07-24, from https://doi.org/10.1021/acs.est.5b01941 doi: 10.1021/acs.est.5b01941

Bandopadhyay, A., Davy, P., & Le Borgne, T. (2018, November). Shear Flows Accelerate Mixing Dynamics in Hyporheic Zones and Hillslopes. *Geophysical Research Letters*, *45*(21), 11,659–11,668. Retrieved 2019-04-10, from http://doi.wiley.com/10.1029/2018GL079914 doi: 10.1029/2018GL079914

Battin, T. J., Besemer, K., Bengtsson, M. M., Romani, A. M., & Packmann, A. I. (2016, April). The ecology and biogeochemistry of stream biofilms. *Nature Reviews Microbiology*, *14*(4), 251–263. Retrieved 2019-04-10, from http://www.nature.com/articles/nrmicro.2016.15 doi: 10.1038/nrmicro.2016.15

Bernhardt, E. S., Rosi, E. J., & Gessner, M. O. (2017, March). Synthetic chemicals as agents of global change. *Frontiers in Ecology and the Environment*, *15*(2), 84–90. Retrieved 2020-07-28, from https://doi.org/10.1002/fee.1450 (Publisher: John Wiley & Sons, Ltd) doi: 10.1002/fee.1450

Boano, F., Packman, A. I., Cortis, A., Revelli, R., & Ridolfi, L. (2007, October). A continuous time random walk approach to the stream transport of solutes: A CTRW APPROACH TO STREAM TRANSPORT. *Water Resources Research*, *43*(10). Retrieved 2019-04-10, from http://doi.wiley.com/10.1029/2007WR006062 doi: 10.1029/2007WR006062

Cheng, F. Y., Preisendanz, H. E., Mashtare, M. L., Lee, L. S., & Basu, N. B. (2021, April). Nevertheless, they persisted: Can hyporheic zones increase the persistence of estrogens in streams? *Water Resources Research*. Retrieved 2021-05-14, from https://onlinelibrary.wiley.com/doi/10.1029/2020WR028518 doi: 10.1029/2020WR028518

Ciparis, S., Iwanowicz, L. R., & Voshell, J. R. (2012, January). Effects of watershed densities of animal feeding operations on nutrient concentrations and estrogenic activity in agricultural streams. *Science of The Total Environment*, *414*, 268–276. Retrieved 2021-05-14, from https://www.sciencedirect.com/science/article/pii/S0048969711011764 doi: 10.1016/j.scitotenv.2011.10.017

Cozzarelli, I. M., Skalak, K. J., Kent, D. B., Engle, M. A., Benthem, A., Mumford, A. C., ... Jolly, G. D. (2017, February). Environmental signatures and effects of an oil and gas wastewater spill in the Williston Basin, North Dakota. *Science of The Total Environment*, *579*, 1781–1793. Retrieved 2021-05-15, from https://www.sciencedirect.com/science/article/pii/S0048969716326201 doi: 10.1016/j.scitotenv.2016.11.157

Dentz, M., Gouze, P., Russian, A., Dweik, J., & Delay, F. (2012, December). Diffusion and trapping in heterogeneous media: An inhomogeneous continuous time random walk approach. *Advances in Water Resources*, *49*, 13–22. Retrieved 2021-04-16, from https://www.sciencedirect.com/science/article/pii/S0309170812002035 doi: 10.1016/j.advwatres.2012.07.015

Dodds, W. K., López, A. J., Bowden, W. B., Stan Gregory, Grimm, N. B., Hamilton, S. K., ... Wilfred Wollheim (2002). N uptake as a function of concentration in streams. *Journal of the North American Benthological Society*, *21*(2), 206–220. Retrieved from https://doi.org/10.2307/1468410 doi: 10.2307/1468410

Fellows, C. S., Valett, H. M., Dahm, C. N., Mulholland, P. J., & Thomas, S. A. (2006, August). Coupling Nutrient Uptake and Energy Flow in Headwater Streams. *Ecosystems*, *9*(5), 788–804. Retrieved 2020-12-22, from https://doi.org/10.1007/s10021-006-0005-5 doi: 10.1007/s10021-006-0005-5

Findlay, S. E. G., Mulholland, P. J., Hamilton, S. K., Tank, J. L., Bernot, M. J., Burgin, A. J., ... Sobota, D. J. (2011, July). Cross-stream comparison of substrate-specific denitrification potential. *Biogeochemistry*, *104*(1), 381–392. Retrieved 2021-05-14, from https://doi.org/10.1007/s10533-010-9512-8 doi: 10.1007/s10533-010-9512-8

Fischer, H. B., List, J. E., Koh, C. R., Imberger, J., & Brooks, N. H. (1979). *Mixing in inland and coastal waters*. Academic press.

Garayburu-Caruso, V. A., Stegen, J. C., Song, H.-S., Renteria, L., Wells, J., Garcia, W., ... Graham, E. B. (2020, May). Carbon Limitation Leads to Thermodynamic Regulation of Aerobic Metabolism. *Environmental Science & Technology Letters*. Retrieved 2020-06-12, from https://doi.org/10.1021/acs.estlett.0c00258 doi: 10.1021/acs.estlett.0c00258

Grant, S. B., Azizian, M., Cook, P., Boano, F., & Rippy, M. A. (2018, March). Factoring stream turbulence into global assessments of nitrogen pollution. *Science*, *359*(6381), 1266–1269. Retrieved 2019-04-10, from http://www.sciencemag.org/lookup/doi/10.1126/science.aap8074 doi: 10.1126/science.aap8074

Grant, S. B., Stewardson, M. J., & Marusic, I. (2012, May). Effective diffusivity and mass flux across the sediment-water interface in streams: EFFECTIVE DIFFUSION COEFFICIENT FOR HYPORHEIC EXCHANGE. *Water Resources Research*, *48*(5). Retrieved 2019-04-10, from http://doi.wiley.com/10.1029/2011WR011148 doi: 10.1029/2011WR011148

Haggerty, R., & Gorelick, S. M. (1995). Multiple-rate mass transfer for modeling diffusion and surface reactions in media with pore-scale heterogeneity. *Water Resources Research*, *31*(10), 2383–2400. (Publisher: Wiley Online Library)

Harvey, J., GomezVelez, J., Schmadel, N., Scott, D., Boyer, E., Alexander, R., ... Choi, J. (2019). How Hydrologic Connectivity Regulates Water Quality in River Corridors. *JAWRA Journal of the American Water Resources Association*, *55*(2), 369–381. Retrieved 2021-05-16, from https://onlinelibrary.wiley.com/doi/abs/10.1111/1752-1688.12691 doi: https://doi.org/10.1111/1752-1688.12691

Harvey, J. W., Bhlke, J. K., Voytek, M. A., Scott, D., & Tobias, C. R. (2013, October). Hyporheic zone denitrification: Controls on effective reaction depth and contribution to whole-stream mass balance: Scaling hyporheic flow controls on stream denitrification. *Water Resources Research*, *49*(10), 6298–6316. Retrieved 2019-04-10, from http://doi.wiley.com/10.1002/wrcr.20492 doi:

10.1002/wrcr.20492

Inwood, S. E., Tank, J. L., & Bernot, M. J. (2007, February). Factors Controlling Sediment Denitrification in Midwestern Streams of Varying Land Use. *Microbial Ecology*, *53*(2), 247–258. Retrieved from https://doi.org/10.1007/s00248-006-9104-2 doi: 10.1007/s00248-006-9104-2

Kelleher, C., Ward, A., Knapp, J. L. A., Blaen, P. J., Kurz, M. J., Drummond, J. D., ... Krause, S. (2019). Exploring Tracer Information and Model Framework Trade-Offs to Improve Estimation of Stream Transient Storage Processes. *Water Resources Research*, *55*(4), 3481–3501. Retrieved 2020-12-22, from https://agupubs.onlinelibrary.wiley.com/doi/abs/10.1029/2018WR023585 (_eprint: https://agupubs.onlinelibrary.wiley.com/doi/pdf/10.1029/2018WR023585) doi: https://doi.org/10.1029/2018WR023585

Khanal, S. K., Xie, B., Thompson, M. L., Sung, S., Ong, S.-K., & van Leeuwen, J. H. (2006, November). Fate, Transport, and Biodegradation of Natural Estrogens in the Environment and Engineered Systems. *Environmental Science & Technology*, *40*(21), 6537–6546. Retrieved 2020-06-10, from https://doi.org/10.1021/es0607739 (Publisher: American Chemical Society) doi: 10.1021/es0607739

Knapp, J. L. A., González-Pinzón, R., Drummond, J. D., Larsen, L. G., Cirpka, O. A., & Harvey, J. W. (2017, February). Tracer-based characterization of hyporheic exchange and benthic biolayers in streams: HYPORHEIC EXCHANGE AND BENTHIC BIOLAYERS. *Water Resources Research*, *53*(2), 1575–1594. Retrieved 2019-04-10, from http://doi.wiley.com/10.1002/2016WR019393 doi: 10.1002/2016WR019393

Krause, S., Lewandowski, J., Grimm, N. B., Hannah, D. M., Pinay, G., McDonald, K., ... others (2017). Ecohydrological interfaces as hot spots of ecosystem processes. *Water Resources Research*, *53*(8), 6359–6376.

Li, A., Aubeneau, A. F., Bolster, D., Tank, J. L., & Packman, A. I. (2017, August). Covariation in patterns of turbulence-driven hyporheic flow and denitrification enhances reach-scale nitrogen removal: HYPORHEIC FLOW-DENITRIFICATION UPSCALING. *Water Resources Research*, *53*(8), 6927–6944. Retrieved 2019-04-10, from http://doi.wiley.com/10.1002/2016WR019949 doi: 10.1002/2016WR019949

O'Connor, B. L., & Harvey, J. W. (2008, December). Scaling hyporheic exchange and its influence on biogeochemical reactions in aquatic ecosystems: HYPORHEIC FLOW AND BIOGEOCHEMICAL REACTIONS. *Water Resources Research*, *44*(12). Retrieved 2019-04-10, from http://doi.wiley.com/10.1029/2008WR007160 doi: 10.1029/2008WR007160

Pia-Ochoa, E., & lvarez Cobelas, M. (2006, October). Denitrification in Aquatic Environments: A Cross-system Analysis. *Biogeochemistry*, *81*(1), 111–130. Retrieved 2021-05-14, from https://doi.org/10.1007/s10533-006-9033-7 doi: 10.1007/s10533-006-9033-7

Reeder, W. J., Quick, A. M., Farrell, T. B., Benner, S. G., Feris, K. P., Marzadri, A., & Tonina, D. (2018). Hyporheic Source and Sink of Nitrous Oxide. *Water Resources Research*, *54*(7), 5001–5016. Retrieved 2020-12-22, from https://agupubs.onlinelibrary.wiley.com/doi/abs/10.1029/2018WR022564 (_eprint: https://agupubs.onlinelibrary.wiley.com/doi/pdf/10.1029/2018WR022564) doi: https://doi.org/10.1029/2018WR022564

Russian, A., Dentz, M., & Gouze, P. (2016). Time domain random walks for hydrodynamic transport in heterogeneous media. *Water Resources Research*, *52*(5), 3309–3323. (Publisher: Wiley Online Library)

Schaper, J. L., Posselt, M., McCallum, J. L., Banks, E. W., Hoehne, A., Meinikmann, K., ... Lewandowski, J. (2018). Hyporheic exchange controls

fate of trace organic compounds in an urban stream. *Environmental science & technology*, *52*(21), 12285–12294. (Publisher: ACS Publications)

Schaper, J. L., Seher, W., Nützmann, G., Putschew, A., Jekel, M., & Lewandowski, J. (2018, September). The fate of polar trace organic compounds in the hyporheic zone. *Water Research*, *140*, 158–166. Retrieved 2020-05-25, from http://www.sciencedirect.com/science/article/pii/S0043135418303348 doi: 10.1016/j.watres.2018.04.040

Tank, J. L., Reisinger, A. J., & Rosi, E. J. (2017). Nutrient Limitation and Uptake. In *Methods in Stream Ecology* (pp. 147–171). Elsevier. Retrieved 2019-04-10, from https://linkinghub.elsevier.com/retrieve/pii/B9780128130476000097 doi: 10.1016/B978-0-12-813047-6.00009-7

Villermaux, J. (1974, December). Deformation of Chromatographic Peaks Under the Influence of Mass Transfer Phenomena. *Journal of Chromatographic Science*, *12*(12), 822–831. Retrieved 2019-04-10, from https://academic.oup.com/chromsci/article-lookup/doi/10.1093/chromsci/12.12.822 doi: 10.1093/chromsci/12.12.822

Voermans, J. J., Ghisalberti, M., & Ivey, G. N. (2018, April). A Model for Mass Transport Across the Sediment-Water Interface. *Water Resources Research*, *54*(4), 2799–2812. Retrieved 2019-04-10, from http://doi.wiley.com/10.1002/2017WR022418 doi: 10.1002/2017WR022418

Ward, A. S., & Packman, A. I. (2019). Advancing our predictive understanding of river corridor exchange. *WIREs Water*, *6*(1), e1327. Retrieved 2020-12-22, from https://onlinelibrary.wiley.com/doi/abs/10.1002/wat2.1327 (_eprint: https://onlinelibrary.wiley.com/doi/pdf/10.1002/wat2.1327) doi: https://doi.org/10.1002/wat2.1327

Zheng, L., & Cardenas, M. B. (2018). Diel Stream Temperature Effects on Nitrogen Cycling in Hyporheic Zones. *Journal of Geophysical Research: Biogeosciences*, *123*(9), 2743–2760. Retrieved 2020-12-22, from https://agupubs.onlinelibrary.wiley.com/doi/abs/10.1029/2018JG004412 (_eprint: https://agupubs.onlinelibrary.wiley.com/doi/pdf/10.1029/2018JG004412) doi: https://doi.org/10.1029/2018JG004412